Absorbing Boundary Conditions in the Frequency-Domain TLM Method and Their Application to Planar Circuits

Damir Pasalic, *Student Member, IEEE,* Jens Bornemann, *Senior Member, IEEE,* and Rüediger Vahldieck, *Fellow, IEEE*

***Abstract*—The frequency-domain transmission-line-matrix method is extended to include absorbing boundary conditions. Three different approaches are considered: zero-reflection termination (ZRT), Berenger's perfectly matched layer (PML), and anisotropic PML. The ZRT technique is the simplest one of the three. Its main advantage over the PML techniques is that it requires no additional nodes to model the boundary. However, when placed too close to an area with high field intensity, the ZRT boundary takes out substantial parts of the transmitted power, thus giving results on the "lossy side." The numerical losses can be reduced by moving the boundaries further away from the area of interest. The PML techniques are more difficult to implement and require additional nodes for their modeling. However, they offer more flexibility since the numerical reflections from the PML absorbers can be controlled by using several layers with conductivities gradually increasing with depth. The computer simulations show that Berenger's and anisotropic PMLs give virtually the same results. A detailed investigation regarding the optimal number of layers in the PML absorbers and distances between the absorbing boundaries and the structure under analysis is performed.**

***Index Terms*—Absorbing boundary conditions, anisotropic PML, Berenger's perfectly matched layer, frequency-domain TLM method, planar circuitry, zero-reflection termination.**

I. Introduction

SINCE ITS introduction by Jin and Vahldieck [1] in 1992, the frequency-domain transmission-line matrix (FDTLM) method has been proven as a versatile numerical tool for eigenvalue and S-parameter analyses of microwave and RF structures of arbitrary shapes. Moreover, utilization of the diakoptics technique in the S-parameter extraction algorithm greatly reduces computer memory and CPU time needed for the calculations. This is especially significant when simulating structures with cascaded discontinuities, such as filters. Thus far, however, open structures simulated with the FDTLM had to be enclosed by metallic or magnetic (M-) walls since absorbing boundaries were not available. Two main disadvantages of this approach are evident: first, metallic and M-walls have to be placed far away from the structure so as not to disturb the electromagnetic (EM) field in the area of interest and, second, artificial waveguide modes are introduced by the metallic and magnetic boundaries. Therefore, in a recent study, we investigated the possibility of implementing absorbing boundary conditions to the FDTLM method. The following two different approaches were considered: zero-reflection termination (ZRT) and anisotropic perfectly matched layer (PML). The two techniques were tested on two-dimensional (2-D) (eigenvalue) and S-parameter analyses of various planar circuits. It was concluded that the ZRT boundaries and the absorbers with only one anisotropic PML provide nearly identical results.

In this paper, we perform a more detailed investigation of the above-mentioned absorbing boundaries. The purpose of this investigation is, first, to provide the design engineer with the specifications of recommended distances between the absorbing boundaries and the structures under analysis and, second, to recommend an appropriate number of PML absorbers. Furthermore, for the first time in literature, we have introduced Berenger's PML [2] to the FDTLM method. While the first two techniques use the already existing FDTLM nodes, the last one requires development of a completely new node to properly model the non-Maxwellian medium of the absorber.

II. Theory

The upper right corner of an FDTLM computational domain is shown in Fig. 1. The computational domain consists of a mesh of symmetrical condensed nodes (SCNs) placed in one slice of the structure under analysis. The EM field inside the computational domain is represented by a set of voltage waves traveling through the mesh along the propagation direction.

The voltage waves are always normally incident to the boundaries and are reflected with reflection coefficient R, e.g., $R = -1$ for a perfect electric conductor (PEC) or $R = +1$ for a perfect M-wall. A lossy conductor boundary is simulated by the appropriate complex reflection coefficient. Open space is simply characterized by $R = 0$, which is why we call this boundary ZRT. We showed in [4] that the ZRT technique can successfully be used in the simulations of many open-boundary problems. The only remaining variable in this approach is the distance of the ZRT walls from the actual circuit.

A completely different approach in simulating absorbing boundaries is the PML technique, originally introduced by Berenger [2] for the termination of FDTD lattices. Since

Manuscript received August 22, 2000; revised January 5, 2001.

D. Pasalic was with the Department of Electrical and Computer Engineering, University of Victoria, Victoria, BC, Canada V8W 3P6. He is now with the Department of Microwave Engineering, Swiss Federal Institute of Technology, CH-8092 Zurich, Switzerland (e-mail: dpasalic@ifh.ee.ethz.ca).

J. Bornemann is with the Department of Electrical and Computer Engineering, University of Victoria, Victoria, BC, Canada V8W 3P6 (e-mail: jbornema@ece.uvic.ca).

R. Vahldieck is with the Laboratory for Electromagnetic Fields and Microwave Electronics, Swiss Federal Institute of Technology, CH-8092 Zurich, Switzerland (e-mail: vah@ifh.ee.ethz.ch).

Publisher Item Identifier S 0018-9480(01)06140-3.

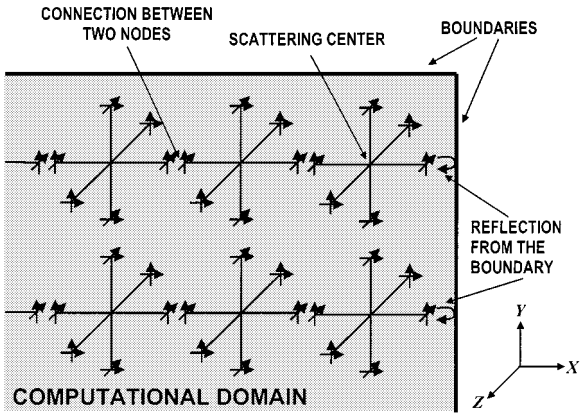

Fig. 1. Discretization mesh of the FDTLM nodes.

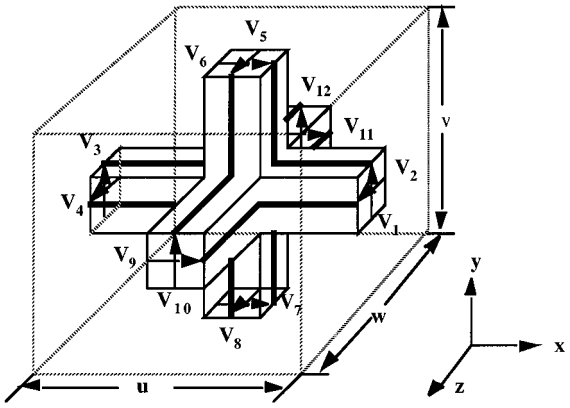

Fig. 2. SCN used in the FDTLM for space discretization.

then, several versions of this technique have been developed in the literature. We focus on Berenger's original PML and Sacks' anisotropic PML [3]. To the best of our knowledge, this is the first time in the literature that Berenger's PMLs are implemented in the FDTLM method.

A. Berenger's PML

Each Cartesian field component in Berenger's PML medium is split into two subcomponents (e.g., $e_x = e_{xy} + e_{xz}$), thus yielding a total of 12 subcomponents related by modified Maxwell's equations (PML equations). However, in this paper, we follow the approach outlined in [6] where the 12 PML equations with split fields are replaced by six PML equations with unsplit fields

$$j\omega\hat{\varepsilon}_y e_x = \frac{\partial h_z}{\partial y} - \frac{\hat{\varepsilon}_y}{\hat{\varepsilon}_z}\cdot\frac{\partial h_y}{\partial z} \tag{1a}$$

$$j\omega\hat{\varepsilon}_z e_y = \frac{\partial h_x}{\partial z} - \frac{\hat{\varepsilon}_z}{\hat{\varepsilon}_x}\cdot\frac{\partial h_z}{\partial x} \tag{1b}$$

$$j\omega\hat{\varepsilon}_x e_z = \frac{\partial h_y}{\partial x} - \frac{\hat{\varepsilon}_x}{\hat{\varepsilon}_y}\cdot\frac{\partial h_x}{\partial y} \tag{1c}$$

$$j\omega\hat{\mu}_y h_x = \frac{\hat{\mu}_y}{\hat{\mu}_z}\cdot\frac{\partial e_y}{\partial z} - \frac{\partial e_z}{\partial y} \tag{1d}$$

$$j\omega\hat{\mu}_z h_y = \frac{\hat{\mu}_z}{\hat{\mu}_x}\cdot\frac{\partial e_z}{\partial x} - \frac{\partial e_x}{\partial z} \tag{1e}$$

$$j\omega\hat{\mu}_x h_z = \frac{\hat{\mu}_x}{\hat{\mu}_y}\cdot\frac{\partial e_x}{\partial y} - \frac{\partial e_y}{\partial x} \tag{1f}$$

where $\hat{\varepsilon}_x$, $\hat{\varepsilon}_y$, $\hat{\varepsilon}_z$, and $\hat{\mu}_x$, $\hat{\mu}_y$, $\hat{\mu}_z$ are complex permittivities and permeabilities of the PML medium corresponding to the x-, y-, and z-directions, respectively. The forms of the complex permittivities and permeabilities are given by

$$\hat{\varepsilon}_i = \varepsilon_0\varepsilon_{ri} - j\frac{\sigma_{ei}}{\omega}$$
$$\hat{\mu}_i = \mu_0\mu_{ri} - j\frac{\sigma_{mi}}{\omega} \tag{2}$$

where $i \in \{x, y, z\}$, ε_{ri}, μ_{ri} are relative permittivities and permeabilities, while σ_{ei} and σ_{mi} are electric and magnetic conductivities of the PML medium. ε_0 and μ_0 are free-space permittivity and permeability.

By following the procedure outlined in [6], [7], we see that the condition for reflectionless transmission of a plane wave from an isotropic lossless medium (ε_r and μ_r) to Berenger's PML medium across the ij-plane interface ($i, j \in \{x, y, z\}$ and $i \neq j$) is given by

$$1 - jk_{im} = 1 - j\cdot\frac{\sigma_{ek}}{\omega\varepsilon_0\varepsilon_r} = 1 - j\cdot\frac{\sigma_{mk}}{\omega\mu_0\mu_r}$$
$$\sigma_{ei} = \sigma_{ej} = 0$$
$$\sigma_{mi} = \sigma_{mj} = 0 \tag{3}$$

where $k \in \{x, y, z\}$ and $k \neq i \neq j$. For simplicity, it is assumed that the x-, y-, and z-direction relative permeabilities and permittivities of the PML medium are equal to those of the isotropic material adjacent to it. Parameter k_{im} determines the rate of wave attenuation in the PML and can be chosen arbitrarily.

In order to model properly Berenger's PML medium with the FDTLM, a new type of SCN has to be derived. As can be seen in Fig. 2, the SCN is a three-dimensional (3-D) transmission-line network. It is completely described by its port scattering matrix $[S_p]$, relating incident and reflected voltages at the ports of the node. The centers of the nodes are grid points, denoted by indexes (i, j, k) in the x-, y-, and z-directions, respectively. Any function of space, i.e., F, at point (i, j, k) is expressed as $F(i, j, k)$.

The port scattering matrix of the new (i.e., PML) node can be derived directly from PML equations (1a)–(1f) by using center differencing and averaging [5]. First, we apply the following transformations:

$$x = u\cdot X$$
$$y = v\cdot Y$$
$$z = w\cdot Z$$
$$e_x = E_x/u$$
$$e_y = E_y/v$$
$$e_z = E_z/w$$
$$h_x = H_x/(uZ_0)$$
$$h_y = H_y/(vZ_0)$$
$$h_z = H_z/(wZ_0). \tag{4}$$

Note that, according to (4), the *normalized* electric and magnetic fields (E_i and H_i, $i \in \{x, y, z\}$), as opposed to the *original* fields (e_i and h_i) in (1a)–(1f) now have the same units (i.e., volt) and, therefore, can be added or subtracted at a later stage of the derivation.

With (4), PML equations (1a)–(1f) simplify to

$$Y_{ey} \cdot E_x = \frac{\partial H_z}{\partial Y} - \frac{\hat{\varepsilon}_y}{\hat{\varepsilon}_z} \cdot \frac{\partial H_y}{\partial Z} \tag{5a}$$

$$Y_{ez} \cdot E_y = \frac{\partial H_x}{\partial Z} - \frac{\hat{\varepsilon}_z}{\hat{\varepsilon}_x} \cdot \frac{\partial H_z}{\partial X} \tag{5b}$$

$$Y_{ex} \cdot E_z = \frac{\partial H_y}{\partial X} - \frac{\hat{\varepsilon}_x}{\hat{\varepsilon}_y} \cdot \frac{\partial H_x}{\partial Y} \tag{5c}$$

$$Z_{my} \cdot H_x = \frac{\hat{\mu}_y}{\hat{\mu}_z} \cdot \frac{\partial E_y}{\partial Z} - \frac{\partial E_z}{\partial Y} \tag{5d}$$

$$Z_{mz} \cdot H_y = \frac{\hat{\mu}_z}{\hat{\mu}_x} \cdot \frac{\partial E_z}{\partial X} - \frac{\partial E_x}{\partial Z} \tag{5e}$$

$$Z_{mx} \cdot H_z = \frac{\hat{\mu}_x}{\hat{\mu}_y} \cdot \frac{\partial E_x}{\partial Y} - \frac{\partial E_y}{\partial X} \tag{5f}$$

where the normalized admittances and impedances are given by

$$Y_{ex} = j\omega\hat{\varepsilon}_x Z_0 \cdot \frac{uv}{w} \tag{6a}$$

$$Y_{ey} = j\omega\hat{\varepsilon}_y Z_0 \cdot \frac{vw}{u} \tag{6b}$$

$$Y_{ez} = j\omega\hat{\varepsilon}_z Z_0 \cdot \frac{uw}{v} \tag{6c}$$

$$Z_{mx} = j\omega\hat{\mu}_x Y_0 \frac{uv}{w} \tag{6d}$$

$$Z_{my} = j\omega\hat{\mu}_y Y_0 \frac{vw}{u} \tag{6e}$$

$$Z_{mz} = j\omega\hat{\mu}_z Y_0 \frac{uw}{v}. \tag{6f}$$

Z_0 and Y_0 are free-space impedance and admittance and u, v, and w are the dimensions of the node in the x-, y-, and z-directions, respectively. Center differencing at point (i, j, k) transforms (5a)–(5f) into a set of finite-difference equations. For example, (5a) is transformed into

$$\begin{aligned} &Y_{ey}E_x(i, j, k) \\ &\quad = \left[H_z\left(i, j + \frac{1}{2}, k\right) - H_z\left(i, j - \frac{1}{2}, k\right)\right] \\ &\qquad - \frac{\hat{\varepsilon}_y}{\hat{\varepsilon}_z} \cdot \left[H_y\left(i, j, k + \frac{1}{2}\right) - H_y\left(i, j, k - \frac{1}{2}\right)\right]. \end{aligned} \tag{7}$$

Similarly, the finite-difference equations corresponding to the rest of (5a)–(5f) can be constructed. The relationships between the normalized field components and the incident and reflected voltage waves at the ports of the SCN are well known from transmission-line theory. For example, for port 1 of the SCN, we have

$$E_y\left(i + \frac{1}{2}, j, k\right) \mp H_z\left(i + \frac{1}{2}, j, k\right) = 2 \cdot V_1^{\text{inc, ref}} \tag{8}$$

where the minus (plus) sign on the left-hand side of the equation corresponds to the incident (reflected) voltage wave. The relationships for the other ports can be found in a similar fashion. By substituting (8) into (7), a set of expressions relating the incident and reflected voltage waves at the ports of the SCN with the normalized field values at the node center is obtained. For example, for $E_x(i, j, k)$, we have

$$\begin{aligned} Y_{ey} \cdot E_x(i, j, k) = {} & V_6^{\text{inc}} - V_6^{\text{ref}} - V_8^{\text{ref}} + V_8^{\text{inc}} - \frac{\hat{\varepsilon}_y}{\hat{\varepsilon}_z} \\ & \cdot \left(V_9^{\text{ref}} - V_9^{\text{inc}} - V_{11}^{\text{inc}} + V_{11}^{\text{ref}}\right). \end{aligned} \tag{9}$$

The next step in the derivation is to express the field variables at the node center (i, j, k) in terms of incident voltages only. This is accomplished by averaging the mixed normalized electric- and magnetic-field components, $(E_x \pm H_y)$, $(E_x \pm H_z)$, $(E_y \pm H_x)$, $(E_y \pm H_z)$, $(E_z \pm H_x)$, and $(E_z \pm H_y)$ along the axes normal to them. For example, the normalized $(E_x + H_y)$ mixed components have the z-axis normal to them, thus, they can be averaged as follows:

$$\begin{aligned} &\left[E_x\left(i, j, k + \frac{1}{2}\right) + H_y\left(i, j, k + \frac{1}{2}\right)\right] \\ &\quad + \left[E_x\left(i, j, k - \frac{1}{2}\right) + H_y\left(i, j, k - \frac{1}{2}\right)\right] \\ &\quad - 2 \cdot \Big[E_x(i, j, k) + H_y(i, j, k)\Big] = 0. \end{aligned} \tag{10}$$

By applying (8) to (10), we obtain another set of equations relating incident and reflected voltages at the ports of the SCN to the normalized field components at the node center. For example, for $(E_x + H_y)$, we have

$$V_9^{\text{ref}} + V_{11}^{\text{inc}} - \Big[E_x(i, j, k) + H_y(i, j, k)\Big] = 0. \tag{11}$$

Similar relations can be found for the other mixed components. Using (9) and (11), one can express the normalized field components at the center of the SCN in terms of the incident voltages at the ports of the node. For the example of E_x and H_y components, we can write

$$\begin{aligned} E_x(i, j, k) &= \frac{2\left(V_6^{\text{inc}} + V_8^{\text{inc}}\right) + 2(\hat{\varepsilon}_y/\hat{\varepsilon}_z)\left(V_9^{\text{inc}} + V_{11}^{\text{inc}}\right)}{Y_{ex} + 2(\hat{\varepsilon}_y/\hat{\varepsilon}_z + 1)} \\ H_x(i, j, k) &= \frac{2\left(V_{11}^{\text{inc}} - V_9^{\text{inc}}\right) + 2(\hat{\mu}_z/\hat{\mu}_x)\left(V_2^{\text{inc}} - V_4^{\text{inc}}\right)}{Z_{my} + 2(\hat{\mu}_z/\hat{\mu}_x + 1)}. \end{aligned} \tag{12}$$

Finally, by substituting (12) for (11), we relate reflected and incident voltages at the ports of the node by

$$\boldsymbol{v}_p^{\text{inc}} = [S_p] \cdot \boldsymbol{v}_p^{\text{ref}} \tag{13}$$

where $\boldsymbol{v}_p^{\text{inc}}$ and $\boldsymbol{v}_p^{\text{ref}}$ are vectors containing the incident and reflected voltages, respectively, at the 12 ports of the SCN. $[S_p]$ is the 12×12 port scattering matrix of the PML node, e.g.,

$$\begin{aligned} S_p(1, 1) &= \frac{2(\hat{\varepsilon}_z/\hat{\varepsilon}_x - 1) - Y_{ez}}{2\left[2(\hat{\varepsilon}_z/\hat{\varepsilon}_x + 1) + Y_{ez}\right]} - \frac{2(1 - \hat{\mu}_x/\hat{\mu}_y) - Z_{mx}}{2\left[2(\hat{\mu}_x/\hat{\mu}_y + 1) + Z_{mx}\right]} \\ S_p(1, 6) &= \frac{2}{2(\hat{\varepsilon}_z/\hat{\varepsilon}_x + 1) + Y_{ez}}. \end{aligned} \tag{14}$$

It is important to notice that the size of the port scattering matrix of the PML node is the same as that of any other regular FDTLM node. Therefore, FDTLM modeling of Berenger's PML medium requires the same computational effort as modeling of any other (Maxwellian) lossy medium.

B. Anisotropic PML

Another type of PML considered in this paper is the anisotropic PML, which was first introduced by Sacks *et al.* [3] in 1995. This approach is based on using a diagonally anisotropic material with specially chosen electric and magnetic properties to describe the absorbing layer. The main advantage of the anisotropic over Berenger's PML is that the former does not require modification of Maxwell's equations. Therefore, no new SCN needs to be derived for modeling the anisotropic PML medium with FDTLM. A short outline of the FDTLM formulation follows. For more details, the reader is referred to [3] and [8].

The source-free formulation of Maxwell's time-harmonic equations in the frequency domain is given by

$$\begin{aligned} \vec{\nabla}\cdot[\hat{\varepsilon}]\vec{e} &= \vec{\nabla}\cdot[\hat{\mu}]\vec{h} = 0 \\ \nabla\times\vec{e} &= -j\omega[\hat{\mu}]\vec{h} \\ \nabla\times\vec{h} &= j\omega[\hat{\varepsilon}]\vec{e} \end{aligned} \tag{15}$$

where $[\hat{\varepsilon}]$ and $[\hat{\mu}]$ are diagonal tensors of the form

$$[\hat{\varepsilon}] = \varepsilon_0 \begin{bmatrix} \varepsilon_{rx} - \dfrac{j\sigma_E^x}{\omega\varepsilon_0} & 0 & 0 \\ 0 & \varepsilon_{ry} - \dfrac{j\sigma_E^y}{\omega\varepsilon_0} & 0 \\ 0 & 0 & \varepsilon_z - \dfrac{j\sigma_E^z}{\omega\varepsilon_0} \end{bmatrix}$$

$$[\hat{\mu}] = \mu_0 \begin{bmatrix} \mu_{rx} - \dfrac{j\sigma_M^x}{\omega\mu_0} & 0 & 0 \\ 0 & \mu_{ry} - \dfrac{j\sigma_M^y}{\omega\mu_0} & 0 \\ 0 & 0 & \mu_{rz} - \dfrac{j\sigma_M^z}{\omega\mu_0} \end{bmatrix}. \tag{16}$$

We consider a situation where a plane wave propagating in an isotropic lossless medium is incident on a material half-space described as a uniaxial anisotropic medium. To match the intrinsic impedances of the isotropic medium (ε_r and μ_r) and the anisotropic half-space ($[\hat{\varepsilon}]$ and $[\hat{\mu}]$), the following condition has to be satisfied:

$$\frac{[\hat{\varepsilon}]}{\varepsilon_0\varepsilon_r} = \frac{[\hat{\mu}]}{\mu_0\mu_r}. \tag{17}$$

Therefore, (16) can be simplified as

$$[\hat{\varepsilon}] = \varepsilon_0\varepsilon_r[\Lambda] = \varepsilon_0\varepsilon_r \begin{bmatrix} a & 0 & 0 \\ 0 & b & 0 \\ 0 & 0 & c \end{bmatrix}$$

$$[\hat{\mu}] = \mu_0\mu_r[\Lambda] = \mu_0\mu_r \begin{bmatrix} a & 0 & 0 \\ 0 & b & 0 \\ 0 & 0 & c \end{bmatrix}. \tag{18}$$

If a boundary between the isotropic medium and the absorbing layer is in the xy-plane, and a plane wave is incident upon it, condition

$$a = b = \frac{1}{c} \tag{19}$$

will ensure reflectionless transmission of the wave into the absorbing layer. To absorb the wave, the absorbing layer must be lossy, i.e., parameters a, b, and c are complex numbers.

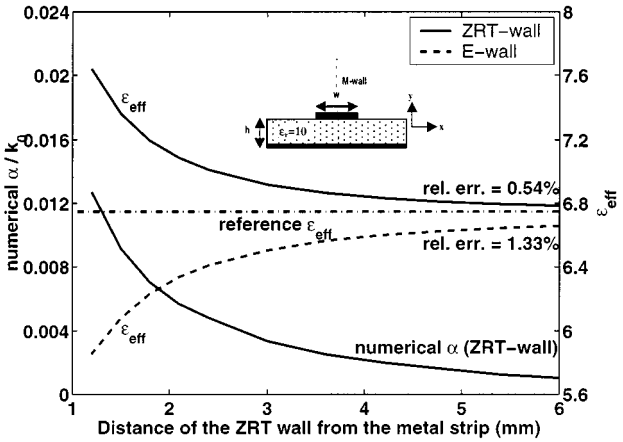

Fig. 3. Results of the 2-D analysis of the microstrip line at 1 GHz. $w = 0.6$ mm, $h = 0.6$ mm, and $\varepsilon_r = 10$.

III. Results

To validate the three approaches, several microstrip and coplanar-waveguide (CPW) structures are selected for comparison with measured data or results obtained with other numerical techniques.

The absorbing boundaries are tested for the 2-D analysis of a microstrip line with conductor width (w) of 0.6 mm and substrate height (h) of 0.6 mm and $\varepsilon_r = 10$. In the simulations, we use M-wall symmetry, while the top and right-hand-side walls are absorbing boundaries. First, ZRT boundaries are used. Fig. 3 shows the results of the 2-D analysis performed at 1 GHz for various distances of the ZRT walls from the metal strip. The reference data is obtained with an in-house SDA code. When the ZRT boundaries are too close to the metal strip (area with high field intensity), they take out (absorb) substantial parts of the transmitted power, thus, numerical losses show up in the results of the 2-D analysis. At the same time, the obtained ε_{eff} is significantly higher than the reference value. As the boundaries are moved further from the strip, the numerical losses decrease, and the calculated ε_{eff} converges toward the reference value. When the ZRT boundaries are placed 6 mm ($\lambda_0/(15\sqrt{\varepsilon_r})$) away from the strip, the calculated ε_{eff} agrees with the SDA solution to within 0.6%, and the normalized numerical α is less than 10^{-3}. For comparison, we also include the ε_{eff} curve calculated with electric (E-) walls used as top and side boundaries. We observe that, similarly to the ZRT boundaries, the convergence is achieved at $\lambda_0/(15\sqrt{\varepsilon_r})$. However, ε_{eff} obtained with E-walls is less accurate than that obtained with ZRT boundaries. Furthermore, when E-walls are used, a number of waveguide modes appear in the 2-D solution. These modes can represent a significant problem in the S-parameter analysis of a microstrip structure with a 3-D discontinuity. On the other hand, when ZRT boundaries are used, the waveguide modes do not appear in the 2-D solution. The nonexistence of the waveguide modes is the main advantage of ZRT boundaries over E-walls. When M-walls are used as the top and side boundaries, the scattering matrices used in the FDTLM algorithm (see [1]) become ill conditioned. Therefore, a reliable eigenvalue analysis with M-walls cannot be performed.

Additional 2-D analyses of microstrip lines performed with ZRT boundaries at higher frequencies lead us to the following conclusion, i.e., the recommended distance of the ZRT boundaries from the metal strip is

$$D \approx \lambda_0 / \left(C \cdot \sqrt{\varepsilon_r}\right) \tag{20}$$

where λ_0 is free-space wavelength and constant C is frequency dependent as follows:

$$C = \begin{cases} 15, & \text{for } 0 < f < 5 \text{ GHz} \\ 7, & \text{for } 5 < f < 10 \text{ GHz} \\ 4, & \text{for } 10 < f < 20 \text{ GHz}. \end{cases}$$

The same microstrip line is simulated with Berenger's PML absorbers used as the top and side boundaries. Although, theoretically, the absorbers should be perfectly reflectionless, some numerical reflections occur due to the finite discretization. To reduce the numerical reflections, the PML absorbers consist of several layers with the electric conductivities increasing with depth according to

$$\sigma_{ei} = \left(\frac{\sum_{j=1}^{i} \Delta_j}{T} \right)^m \sigma_{\max} \tag{21}$$

where i is the layer number, Δ_j's are the thicknesses of the layers, T is the total thickness of the absorber, and $\sigma_{\max}$ is the maximal electric conductivity. Parameter m controls the rate of increase of the conductivities of the successive layers and can be set arbitrarily. The magnetic conductivities of the layers are matched to the corresponding electric conductivities according to (3). For example, the side PMLs, normal to the x-direction, have σ_{ex} and σ_{mx} matched according to (3) and the conductivities in the other two directions set to zero. In the corner region, where there is an overlap of the top and side PMLs, both x- and y-directions conductivities are present and set equal to those of the adjacent PMLs. The z-direction conductivities in the corner PML regions are still zero.

Calculated ε_{eff}s for different distances between the absorbers and the metal strip are shown in Fig. 4. For comparison, we include the results obtained with Berenger's PML absorbers with one and three layers, ZRT boundaries, as well as reference data obtained with the SDA method. For the PML absorbers, we set $\sigma_{\max} = 50$ S/m and parameter $m = 4$. We see that the PML absorber with only a single layer gives almost identical results to those obtained with ZRT boundaries, which confirms our findings in [4].

By increasing the number of layers in the PML absorber, its performance is significantly improved. This can be explained by the fact that a larger number of layers with gradually increased conductivities creates less abrupt transitions between the isotropic material and the first PML, as well as between the PMLs inside the absorber. Consequently, the numerical reflection between the isotropic material and the PML absorber is decreased. In Fig. 4, we can see that the PML absorbers with three layers can be placed approximately 3 mm ($\lambda_0/(30 \cdot \sqrt{\varepsilon_r})$) away from the metal strip for sufficient accuracy. Analyses performed for other planar structures and frequencies have confirmed that the optimum number of layers in a Berenger's PML

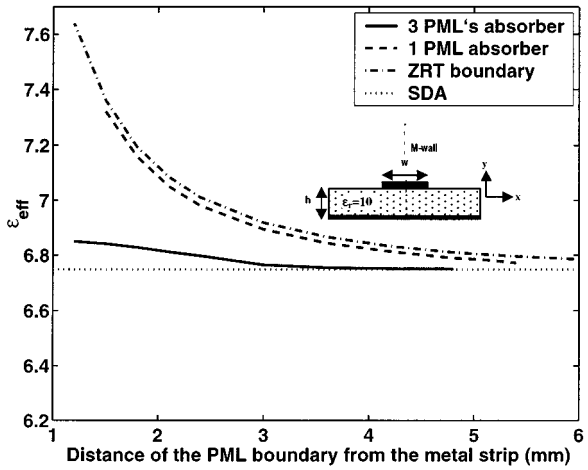

Fig. 4. Effective permittivity of the microstrip line at 1 GHz. $h = 0.6$ mm, 0.6 mm, and $\varepsilon_r = 10$.

absorber is three, maximal conductivity is 50 S/m, and parameter $m = 4$. The recommended distance between the absorber and metal strip can be set according to

$$D \approx \lambda_0 / \left(C \cdot \sqrt{\varepsilon_r}\right) \tag{22}$$

where

$$C = \begin{cases} 30, & \text{for } 0 < f < 5 \text{ GHz} \\ 14, & \text{for } 5 < f < 10 \text{ GHz} \\ 8, & \text{for } 10 < f < 20 \text{ GHz}. \end{cases}$$

As explained in [6], anisotropic and Berenger's PMLs are mathematically equivalent. Therefore, we expect the two techniques to provide the same results. This is confirmed at the example of a microstrip line with a lossless dielectric substrate with relative permittivity of $\varepsilon_r = 4$. The thickness of the substrate is $h = 0.5$ mm and the strip width $w = 1$ mm. Effective permittivity curves, for the frequency range of 1–30 GHz, are calculated with both techniques. The FDTLM simulation is carried out with PML absorbers with three layers placed 5 mm from the strip. This distance corresponds to $\lambda_0/(30\sqrt{\varepsilon_r})$ at 1 GHz. Conductivities of the layers are calculated from (21) with $\sigma_{\max} = 50$ S/m and $m = 4$. When Berenger's PML is used, the medium in the corner region has z-direction conductivities set to zero, and x- and y-directions conductivities equal to those of the adjacent PMLs. In the case of anisotropic PML absorbers, the permittivity and permeability tensors of the PML medium are given by (18). For the PMLs in the top and side absorbers, parameters a, b, and c follow condition (19) in the appropriate form. For example, for the top absorber, the parameters have the following relationship: $a = 1/b = c$. The values of parameters a, b, and c for the corner regions are obtained by using a more general expression for matrix $[\Lambda]$ given by

$$[\Lambda] = \begin{bmatrix} \frac{s_y s_z}{s_x} & 0 & 0 \\ 0 & \frac{s_x s_z}{s_y} & 0 \\ 0 & 0 & \frac{s_x s_y}{s_z} \end{bmatrix} \tag{23}$$

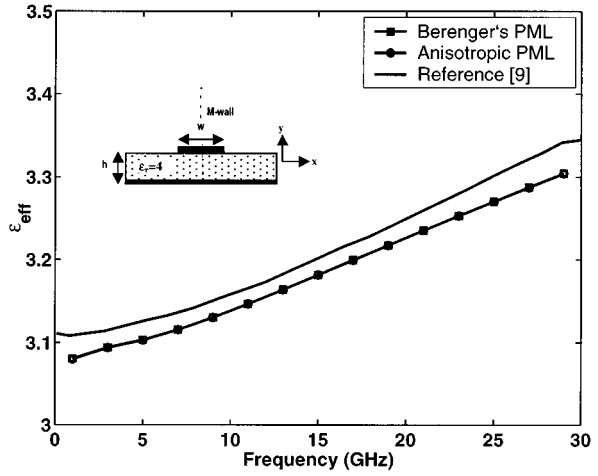

Fig. 5. Frequency-dependent ε_{eff} of the microstrip line with $h = 0.5$ mm, $w = 1$ mm, and $\varepsilon_r = 4$.

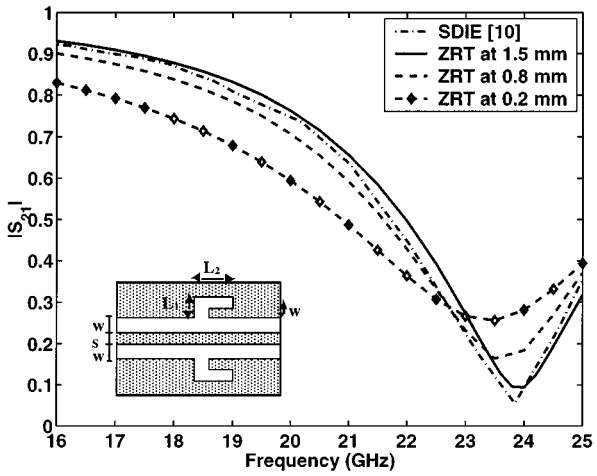

Fig. 6. Transmission coefficient of the CPW resonator with L-shaped series stubs. $w = 0.225$ mm, $s = 0.45$ mm, $L_1 = 0.45$ mm, and $L_2 = 1.125$ mm. Substrate thickness $h = 0.635$ mm and $\varepsilon_r = 9.9$.

where $s_i = 1 - j\sigma_{ei}/(\omega\varepsilon_0\varepsilon_r)$, $i \in \{x, y, z\}$. This expression can be derived by using the mathematical equivalence of the Berenger's and anisotropic PMLs. Due to lack of space, the derivation is not presented here; however, a more interested reader is referred to [6] and [8]. One should note that parameters a, b, and c in the noncorner regions can be obtained from (23) by setting s_i's in the appropriate directions to unity. For example, by setting $s_x = s_z = 1$, we obtain parameters a, b, and c of the top absorber's PMLs. In the corner region, s_z is set to one, while s_x and s_y are equal to those of the adjacent side and top PMLs, respectively.

The calculated ε_{eff} curves together with the reference data taken from [9] are shown in Fig. 5. The required number of nodes in the computational domain is 18×18, including the nodes in the absorber. As predicted, the simulations with anisotropic and Berenger's PMLs give virtually identical results. The two techniques agree to within three decimal points. The FDTLM results are in excellent agreement with the reference data, obtained with the FDTD method in a computational domain of 210×80 cells. The difference between the ε_{eff} curves obtained with FDTLM and FDTD is less than 1%. Since Berenger's and anisotropic PMLs give virtually identical results and there is no difference in computational effort required for modeling the two media, they will not be distinguished in this paper. They will be referred to simply as the PML.

The PML and ZRT boundaries are tested for S-parameter analysis of a CPW resonator with L-shaped series stubs whose mean lengths are 1.35 mm. The primary objective of the performed tests is to determine a sufficient distance between the absorbing boundaries and the structure under analysis. The geometry of the resonator and its transmission coefficient calculated with ZRT boundaries are shown in Fig. 6. To reduce the computational effort, we apply an M-wall condition in the symmetry plane. The absorbing boundaries are placed at the top, bottom, and right-hand side of the structure. We also include the reference data [10] obtained with the space domain integral equation (SDIE) technique. In order to arrive at accurate results, the ZRT boundaries have to be placed approximately 1.5 mm from

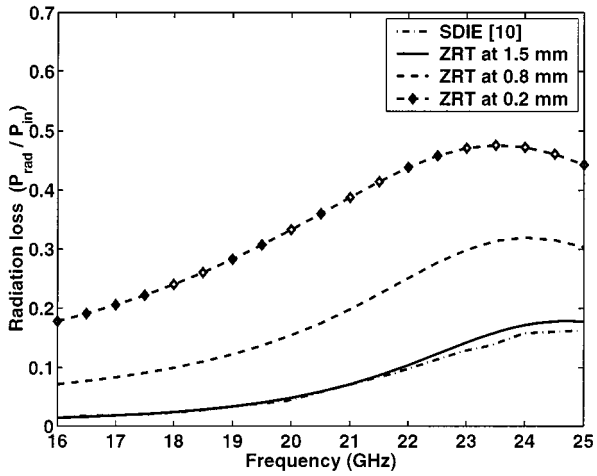

Fig. 7. Radiation loss $1-|S_{11}|^2-|S_{21}|^2$ of the CPW resonator with L-shaped series stubs.

the resonator. This distance corresponds to $\lambda_0/(4\sqrt{\varepsilon_r})$, which is the recommended distance for the microstrip at 16 GHz, given by (20). We see that the recommendations given for microstrip circuits can be used for CPW structures as well. The calculated radiation loss for the CPW resonator with bent series stubs is shown in Fig. 7. Excellent agreement between the FDTLM and SDIE is achieved when the ZRT boundaries are placed 1.5 mm from the CPW structure.

The PML absorber used in the simulations consists of three layers with electric conductivities increasing with depth, as given by (21). The maximum conductivity is set to $\sigma_{\max} = 50$ S/m and parameter $m = 4$. The conductivities of the absorber's layers, including the corner regions, are set in the fashion described in the examples of the microstrip lines of Figs. 4 and 5. The distances between the absorbers and the CPW structure are half the distances used for the ZRT boundaries. Fig. 8 compares the calculated transmission coefficient with the reference data [10]. A very good agreement between the FDTLM and SDIE results is achieved when the PML absorbers are placed 0.8 mm from the CPW structure. As

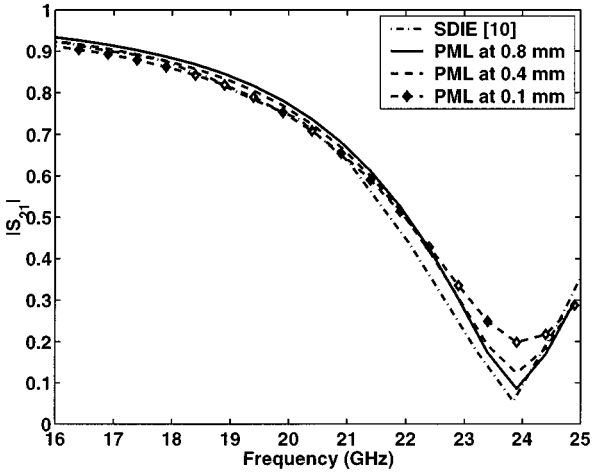

Fig. 8. Transmission coefficient of the CPW resonator with L-shaped stubs. PML absorbers are used as the absorbing boundaries.

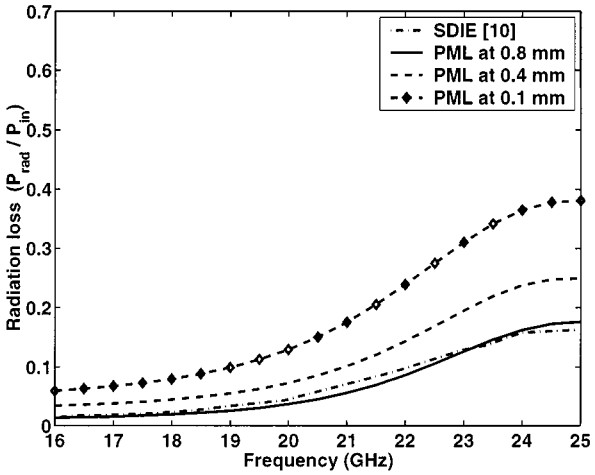

Fig. 9. Radiation loss $1 - |S_{11}|^2 - |S_{21}|^2$ of the CPW resonator with L-shaped series stubs obtained for various distances between the PML absorber and resonator structure.

in the case of ZRT boundaries, this distance corresponds to the recommended distance for microstrip circuits (22).

The radiation loss of the resonator calculated for various distances between the PML absorber and CPW structure is shown in Fig. 9. When the boundaries are placed 0.8 mm from the resonator, we obtain excellent agreement between the FDTLM and reference data. From Figs. 7 and 9, we see that the calculated radiation is increased when the absorbing boundaries are placed too close to the resonator. Accordingly, the minimum of the transmission coefficient gets less sharp. This effect can be explained by a *forced radiation* induced by absorbing boundaries placed too close to the areas of high field concentration.

Finally, the FDTLM with ZRT and PML boundaries is used to analyze the asymmetrically edge-fed patch antenna [11], which is illustrated in Fig. 10. The absorbing boundaries are placed according to (20) and (22) for the lowest frequency (i.e., 5 GHz). The comparison of the FDTLM results with the experimental data taken from [11] is shown in Fig. 10. The FDTLM correctly predicts the general shape of the return loss. The resonant

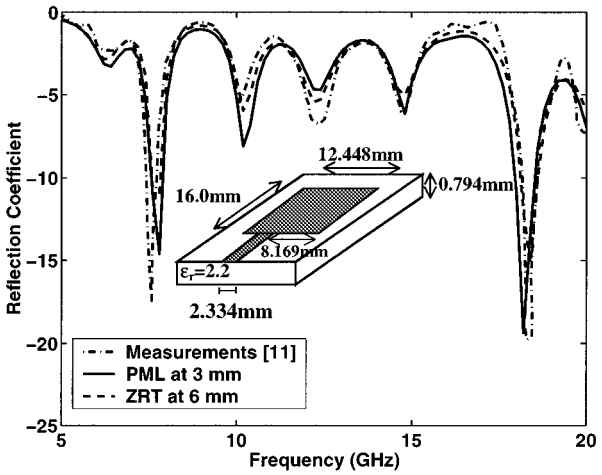

Fig. 10. Frequency-dependent reflection coefficient of the asymmetrically edge-fed patch antenna. Comparison of the FDTLM with PML and ZRT with experimental data.

frequencies are in perfect agreement with the measured data. However, slight differences between the modeled and measured curves occur. For example, a fine ripple occurs in the measurement at about 17.5 GHz due to some problems with the measurement setup, as discussed in detail in [11]. Additionally, some parameters, such as dielectric and conductor losses, are not included in the simulation, which further contributes to the discrepancy between the theory and experiment.

IV. Conclusions

A very efficient implementation of open boundary conditions into the FDTLM method has been presented. The easy-to-implement ZRT technique utilizes the unique way of field representation in the TLM method. Its main advantage is that it requires no additional nodes to model the boundary. However, if ZRT walls are placed too close to the structure area with high field intensity, they absorb the transmitted power, thus creating unwanted numerical losses. The only way of reducing the losses it to move the ZRT walls further from the area of interest. The PML absorbers are more complicated to implement and require additional nodes for their modeling. However, they provide more flexibility than ZRT boundaries since the numerical reflections from the PML absorbers can be decreased without moving the absorbers far away from the areas with high field intensity. The numerical reflections can be reduced by increasing the number of layers in the PML absorbers. Computer simulations demonstrate that Berenger's and anisotropic PMLs give virtually the same results and that absorbers with three layers are sufficient for accurate analyses of most planar circuits. The distance between the absorbing boundaries and the structure under analysis should approximately be half as large for the PML absorbers as for the ZRT boundaries.

Acknowledgment

The authors would like to thank Dr. S. Amari, University of Victoria, Victoria, BC, Canada, for his help in obtaining the SDA reference data for the microstrip lines of Figs. 3 and 4.

REFERENCES

[1] H. Jin and R. Vahldieck, "The frequency-domain transmission line matrix method—A new concept," *IEEE Trans. Microwave Theory Tech.*, vol. 40, pp. 2207–2218, Dec. 1992.

[2] J.-P. Berenger, "A perfectly matched layer for the absorption of electromagnetic waves," *J. Comput. Phys.*, vol. 114, pp. 185–200, Oct. 1994.

[3] Z. S. Sacks, D. M. Kingsland, R. Lee, and J. F. Lee, "A perfectly matched anisotropic absorber for use as an absorbing boundary condition," *IEEE Trans. Antennas Propagat.*, vol. 43, pp. 1460–1463, Dec. 1995.

[4] D. Pasalic, R. Vahldieck, and J. Hesselbarth, "Frequency-domain TLM method with absorbing boundary conditions," in *IEEE MTT-S Int. Microwave Symp. Dig.*, 1999, pp. 1669–1672.

[5] H. Jin and R. Vahldieck, "A new frequency-domain TLM symmetrical condensed node derived directly from Maxwell's equations," in *IEEE MTT-S Int. Microwave Symp. Dig.*, 1995, pp. 487–490.

[6] R. Mittra and U. Pekel, "A new look at the perfectly matched layer (PML) concept for the reflectionless absorption of electromagnetic waves," *IEEE Microwave Guided Wave Lett.*, vol. 5, pp. 84–86, Mar. 1995.

[7] U. Pekel and R. Mittra, "An application of the perfectly matched layer (PML) concept to the finite element method frequency domain analysis of scattering problems," *IEEE Microwave Guided Wave Lett.*, vol. 5, pp. 258–260, Aug. 1995.

[8] S. D. Gedney, "An anisotropic perfectly matched layer—Absorbing medium for the truncation of FDTD lattices," *IEEE Trans. Antennas Propagat.*, vol. 44, pp. 1630–1639, Dec. 1996.

[9] Z. Wu and J. Fang, "Numerical implementation and performance of perfectly matched layer boundary condition for waveguide structures," *IEEE Trans. Microwave Theory Tech.*, vol. 43, pp. 2676–2683, Dec. 1995.

[10] N. I. Dib, W. P. Harokopus, Jr., G. E. Ponchak, and L. P. B. Katehi, "A comparative study between shielded and open coplanar waveguide discontinuities," *Int. J. Microwave Millimeter-Wave Computer-Aided Eng.*, vol. 2, no. 4, pp. 331–341, 1992.

[11] S.-C. Wu, N. G. Alexopoulos, and O. Fordham, "Feeding structure contribution to radiation by patch antennas with rectangular boundaries," *IEEE Trans. Antennas Propagat.*, vol. 40, pp. 1245–1249, Oct. 1992.

Damir Pasalic (S'98) was born in Sarajevo, Bosnia Herzegovina, in June 1972. He received the B.Eng. and M.A.Sc. degrees in electrical engineering from the University of Victoria, Victoria, BC, Canada, in 1999 and 2000, respectively, and is currently working toward the Ph.D. degree in microwave engineering at the Swiss Federal Institute of Technology, Zurich, Switzerland.

From 1996 to 1999, he was a Junior Research Assistant in the Department of Electrical and Computer Engineering, University of Victoria. His research interests include numerical modeling and design of microwave, millimeter-wave, and opto-electronic integrated circuits.

Jens Bornemann (M'87–SM'90) received the Dipl.-Ing. and the Dr.-Ing. degrees in electrical engineering from the University of Bremen, Bremen, Germany, in 1980 and 1984, respectively.

From 1984 to 1985, he was a Consulting Engineer. In 1985, he joined the University of Bremen as an Assistant Professor. Since April 1988, he has been with the Department of Electrical and Computer Engineering, University of Victoria, Victoria, BC, Canada, where he became a Professor in 1992. From 1992 to 1995, he was a Fellow of the British Columbia Advanced Systems Institute. In 1996, he was a Visiting Scientist at Spar Aerospace Limited, Ste-Anne-de-Bellevue, QC, Canada, and a Visiting Professor in the Microwave Department, University of Ulm, Ulm, Germany. Since 1997, he has been a Co-Director of the Center for Advanced Materials and Related Technology (CAMTEC), University of Victoria. He co-authored *Waveguide Components for Antenna Feed Systems: Theory and CAD* (Norwood, MA: Artech House, 1993) and has authored/co-authored over 170 technical papers. His research activities include microwave/millimeter-wave components and systems design, and problems involving EM-field theory in integrated circuits, waveguide feed networks, and radiating structures. He serves on the Editorial Advisory Board of the *International Journal of Numerical Modeling*.

Dr. Bornemann is a Registered Professional Engineer in the Province of British Columbia, Canada. He is a Senior Member of the IEEE Microwave Theory and Techniques Society (IEEE MTT-S) and the IEEE Antennas and Propagation Society (IEEE AP-S). He was a corecipient of the A. F. Bulgin Premium of the Institution of Electronic and Radio Engineers in 1983. He currently serves as an associate editor for the IEEE TRANSACTIONS ON MICROWAVE THEORY AND TECHNIQUES in the area of microwave modeling and computer-aided design (CAD) and on the Technical Program Committee of the IEEE MTT-S International Microwave Symposium.

Rüdiger Vahldieck (M'85–SM'86–F'99) received the Dipl.-Ing. and Dr.-Ing. degrees in electrical engineering from the University of Bremen, Bremen, Germany, in 1980 and 1983, respectively.

From 1984 to 1986, he was a Research Associate at the University of Ottawa, Ottawa, ON, Canada. In 1986, he joined the Department of Electrical and Computer Engineering, University of Victoria, Victoria, BC, Canada, where he became a Full Professor in 1991. During the fall and spring of 1992–1993, he was a Visiting Scientist at the Ferdinand-Braun-Institute für Hochfrequenztechnik, Berlin, Germany. Since 1997, he has been a Professor of field theory at the Swiss Federal Institute of Technology, Zurich, Switzerland. Since 1981, he has authored or co-authored over 170 technical papers in books, journals, and conferences, mainly in the field of microwave CAD. His research interests include numerical methods to model EM fields in the general area of electromagnetic compatibility (EMC) and, in particular, for CAD of microwave, millimeter-wave, and opto-electronic integrated circuits.

Prof. Vahldieck was the president of the IEEE 2000 International Zurich Seminar on Broadband Communications (IZS'2000) and vice president of the EMC Congress, Zurich, Switzerland. He is a member of the editorial board of the IEEE TRANSACTIONS ON MICROWAVE THEORY AND TECHNIQUES and an associate editor of the *IEEE Microwave and Guided Wave Letters*. Since 1992, he has been on the Technical Program Committee of the IEEE Microwave Theory and Techniques Society (IEEE MTT-S) International Microwave Symposium, the IEEE MTT-S Technical Committee on Microwave Field Theory, and in 1999, on the Technical Program Committee of the European Microwave Conference. Professor Vahldieck is currently the chairman of the IEEE Swiss Joint Chapter on Microwave Theory and Techniques, Antennas and Propagation, and Electromagnetic Compatibility. Together with three co-authors, he received the 1983 Outstanding Publication Award of the Institution of Electronic and Radio Engineers. In 1996, he received the J. K. Mitra Award of the Institution of Electronics and Telecommunications Engineers for the best research paper of 1995.